

Model-independent determination of the cosmic growth factor

Sophia Haude^{1*}, Shabnam Salehi¹, Sofia Vidal¹,
Matthias Bartelmann² and Matteo Maturi^{1,2}

¹ Institute for Theoretical Astrophysics, ZAH, Heidelberg University, Germany

² Institute for Theoretical Physics, Heidelberg University, Germany

* sophiahaude@gmx.de

Abstract

The two most important functions describing the evolution of the universe and its structures are the expansion function $E(a)$ and the linear growth factor $D_+(a)$. It is desirable to constrain them based on a minimum of assumptions in order to avoid biases from assumed cosmological models. The expansion function has been determined in previous papers in a model-independent way using distance moduli to type-Ia supernovae and assuming only a metric theory of gravity, spatial isotropy and homogeneity. Here, we extend this analysis in three ways: (1) We enlarge the data sample by combining measurements of type-Ia supernovae with measurements of baryonic acoustic oscillations; (2) we substantially simplify and generalise our method for reconstructing the expansion function; and (3) we use the reconstructed expansion function to determine the linear growth factor of cosmic structures, equally independent of specific assumptions on an underlying cosmological model other than the usual spatial symmetries. In this approach, the present-day matter-density parameter Ω_{m0} is the only relevant parameter for an otherwise purely empirical and accurate determination of the growth factor. We further show how our method can be used to derive a possible time evolution of the dark energy as well as the growth index directly from distance measurements. Deviations from Λ CDM that we see in some of our results may be due to possibly insufficient flexibility of our method that could be cured by larger data samples, a real departure from Λ CDM at $a \lesssim 0.3$, or hidden systematics in the data. The latter could be a matter of concern for all type-Ia supernovae analyses based on Λ CDM fitting approaches, especially in view of the current dispute on the value of H_0 . These results illustrate the applicability of our approach as a diagnostic tool.



Copyright S. Haude *et al.*

This work is licensed under the Creative Commons

[Attribution 4.0 International License](https://creativecommons.org/licenses/by/4.0/).

Published by the SciPost Foundation.

Received 11-12-2019

Accepted 20-10-2021

Published 17-01-2022

doi:[10.21468/SciPostAstro.2.1.001](https://doi.org/10.21468/SciPostAstro.2.1.001)

1

2 Contents

3	1 Introduction	2
4	2 Cosmic expansion	3
5	2.1 Method	3
6	2.2 Cosmic expansion function from the SN sample	5
7	2.3 Cosmic expansion function from the SN-BAO sample	6

8	3 Linear growth of cosmic structures	9
9	3.1 Equation to be solved	9
10	3.2 Initial conditions and results for the linear growth factor	9
11	3.3 The growth index of linear perturbations	10
12	4 Comparison of different data samples	11
13	5 Conclusions	14
14	A Chebyshev polynomials	15
15	B Derivation of the growth index	15
16	C BAO sample	16
17	References	20
18	<hr/>	
19		

20 1 Introduction

21 The expansion function of the universe and the linear growth factor of cosmic structures
22 are the two most fundamental functions describing the evolution of the universe and its
23 structures. They are indirectly accessible to astronomical observations, such as luminosity-
24 distance measurements of type-Ia supernovae (SN Ia). Combining both functions allows to
25 distinguish between different cosmological models.

26 The accelerated expansion rate of the universe has been established more than twenty
27 years ago based on SN Ia distance measurements [1, 2]. The cosmological standard model
28 explains this acceleration by the cosmological constant or a dynamical dark-energy component
29 currently dominating the energy content of the universe [3]. The nature of the dark energy is
30 largely unknown. So far, all attempts to derive it from fundamental theory have led to values
31 which are way too large to explain the cosmic acceleration. Phenomenological explanations
32 are typically based on a dark-energy equation of state, possibly varying with time. Some of
33 them bypass fine-tuning problems, but lack fundamental justifications. Constraining the nature
34 of the dark energy thus remains one of the most important tasks for contemporary cosmology.
35 The two functions mentioned, the cosmic expansion function and the linear growth factor of
36 cosmic structures, are the most important links between observations and the nature of the
37 dark energy.

38 We are here proposing a method to constrain the linear growth factor of cosmic structures
39 without reference to any specific model for the energy content of the universe. We derive the
40 expansion function in a way similar to that proposed by [4] and [5], but in a substantially
41 simplified and standardised manner. The only assumptions made there are that the universe is
42 topologically simply connected, spatially homogeneous and isotropic on average, and that the
43 expansion rate is reasonably smooth. Extending this analysis to the linear growth of cosmic
44 structures, we only add the assumption that the linear growth of cosmic structures on the
45 relevant scales is locally driven by Newtonian gravity.

46 We briefly review and revise the method of [4] in Sect. 2 and apply it exemplarily to the
47 Pantheon sample of type-Ia supernovae (SN sample hereafter) and to the Pantheon sample
48 combined with a sample of distance measurements from baryonic acoustic oscillations (BAO,
49 hereafter SN-BAO sample) to obtain a purely empirical and rather tight constraint of the cosmic

50 expansion function. We further show how, assuming a spatially flat Friedmann-Lemaître model
 51 with dynamical dark energy, the hypothetical time evolution of dark energy can be derived
 52 from the empirically determined expansion function. In Sect. 3 we describe our method to
 53 calculate the linear growth factor, discuss the initial conditions for solving the growth equation,
 54 and present the results obtained from the SN sample and the SN-BAO sample. As an additional
 55 application we show how to derive the growth index from the expansion function. In Sect. 4,
 56 we briefly discuss the dependence of the derived functions on the data sample in view of
 57 controversies in the literature about the acquisition of existing SN samples. We illustrate the
 58 incompatibilities between two such samples by applying our method to both. Some of our
 59 derived functions deviate significantly from the Λ CDM predictions for both data samples, and
 60 we discuss possible reasons and implications. Finally, we summarise our conclusions in Sect. 5.

61 2 Cosmic expansion

62 2.1 Method

63 As outlined in [4], the expansion function can be deduced from the luminosity of light sources of
 64 known intrinsic luminosity, such as calibrated SNe Ia, without assuming any specific Friedmann-
 65 Lemaître model. We briefly review this method in this section in a modified, simplified, and
 66 standardised version.

67 Even though gravity is commonly described by general relativity (GR), we only need to
 68 assume that space-time is described by a metric theory of gravity. We thus treat space-time as a
 69 four-dimensional, differentiable manifold with a metric tensor g . Assuming spatial isotropy
 70 and homogeneity, this metric has to be of the Robertson-Walker form with a scale factor a . In
 71 general relativity, Einstein's field equations applied to the Robertson-Walker metric turn into the
 72 Friedmann equations, and the metric further specialises to the Friedmann-Lemaître-Robertson-
 73 Walker form. Then, the cosmic expansion function $E(a)$ is given in terms of the Hubble function
 74 $H(a)$ by

$$\begin{aligned} H^2(a) &= H_0^2 (\Omega_{r0} a^{-4} + \Omega_{m0} a^{-3} + \Omega_{DE}(a) + \Omega_{K0} a^{-2}) \\ &=: H_0^2 E^2(a). \end{aligned} \quad (1)$$

75 This defines the cosmic expansion function $E(a)$ in terms of the Hubble constant H_0 and the
 76 contributing energy-density parameters. These are the radiation density Ω_{r0} , the matter density
 77 Ω_{m0} , the density parameter Ω_{K0} of the spatial curvature, all at the present time, and the possibly
 78 time-dependent dark-energy density parameter $\Omega_{DE}(a)$. In the standard Λ CDM cosmology, Ω_{DE}
 79 is replaced by the cosmological constant with the density parameter $\Omega_{\Lambda 0}$ at the present time.

80 It is important in our context that we do *not* assume any specific parameterisation of
 81 the expansion function of the type (1). Rather, we merely assume that we can build upon
 82 an underlying, but unspecified metric theory of gravity with the two common symmetry
 83 assumptions of spatial isotropy and homogeneity. The metric must then be of Robertson-Walker
 84 form, and its single remaining degree of freedom must be described by some expansion function
 85 $E(a)$ whose form is *a priori* undetermined. We reconstruct $E(a)$ from data without adopting
 86 the parameterisation (1).

87 As an uncritical simplification, we further assume that the spatial sections of the space-time
 88 manifold are flat, following the empirical evidence for the spatial curvature of our Universe to
 89 be indistinguishable from zero within the limits of our observational uncertainties [6]. It would
 90 be quite straightforward to extend our analysis by replacing the radial comoving distance w in
 91 Eq. (9) below by the comoving angular-diameter distance $f_K(w)$.

92 We modify the approach developed in [4, 5] and used in [7, 8] in two important ways,
 93 allowing a substantial simplification and rendering the results more portable than before. First,
 94 we use Chebyshev polynomials of the first kind $T_n(x)$, shifted to the interval $[0, 1]$, as an
 95 orthonormal basis-function system (see Appendix A). Second, we do not expand the distance,
 96 but a scaled variant of the inverse expansion function $E(a)$ into these polynomials.

97 Given measurements of distance moduli μ_i and redshifts z_i , with $1 \leq i \leq N$, we convert the
 98 distance moduli to luminosity distances $D_{\text{lum},i}$ via

$$D_{\text{lum},i} = 10^{1+0.2\mu_i} \text{ pc} \quad (2)$$

99 and scale the redshifts z_i to the variable

$$x_i := \frac{a_i - a_{\min}}{1 - a_{\min}}, \quad a_i = (1 + z_i)^{-1}, \quad (3)$$

100 normalised to the interval $[0, 1]$, where $a_{\min} = (1 + z_{\max})^{-1}$ is the scale factor of the maximum
 101 redshift in the sample. We further introduce the scaled luminosity distance

$$d_i = a_{\min}^2 (1 + \delta a x_i) D_{\text{lum},i}, \quad \delta a := \frac{1 - a_{\min}}{a_{\min}}. \quad (4)$$

102 Since the uncertainties on the redshifts are very small compared to those of the distance, the
 103 relative uncertainty of d_i is unchanged compared to that of $D_{\text{lum},i}$. We thus obtain a scaled data
 104 sample $\{x_i, d_i\}$.

105 The radial comoving coordinate is

$$w(x) = \int_t^{t_0} \frac{cdt'}{a(t')} = \int_x^1 \frac{cdx'}{a(x')\dot{x}'} = \int_x^1 \frac{cdx'}{a_{\min}\dot{x}'(1 + \delta a x')}, \quad (5)$$

106 in terms of the normalised scaled factor x . We define

$$e(x) := [\dot{x}(1 + \delta a x)]^{-1} \quad (6)$$

107 and use

$$\dot{x} = \frac{\dot{a}}{a_{\min} \delta a} = \frac{\dot{a}}{a} \frac{a}{a_{\min} \delta a} = H_0 E(a) \frac{1 + \delta a x}{\delta a} \quad (7)$$

108 to write $e(x)$ as

$$e(x) = \frac{\delta a}{E(a)(1 + \delta a x)^2}. \quad (8)$$

109 The luminosity distance in units of the Hubble radius c/H_0 is

$$D_{\text{lum}}(x) = \frac{w(x)}{a(x)} = \frac{1}{a_{\min}^2 (1 + \delta a x)} \int_x^1 dx' e(x'), \quad (9)$$

110 in spatially-flat geometry, using $a = a_{\min}(1 + \delta a x)$. Thus, the scaled luminosity distance $d(x)$ is

$$d(x) = \int_x^1 dx' e(x'), \quad (10)$$

111 and the scaled, inverse expansion function $e(x)$ is its negative derivative,

$$e(x) = -d'(x). \quad (11)$$

112 We now proceed as follows with the transformed data set $\{x_i, d_i\}$. We expand $e(x)$ into shifted
 113 Chebyshev polynomials $T_n^*(x)$,

$$e(x) = \sum_{j=1}^M c_j T_j^*(x). \quad (12)$$

114 Then, the scaled distances $d(x)$ are given by

$$d(x) = \sum_{j=1}^M c_j p_j(x), \quad p_j(x) := \int_x^1 dx' T_j^*(x'). \quad (13)$$

115 Defining the matrix P by its components

$$P_{ij} := p_j(x_i), \quad 1 \leq i \leq N, \quad 1 \leq j \leq M, \quad (14)$$

116 the vector \vec{c} of coefficients c_j is determined by the data vector $\vec{d} = (d_i)^\top$ via

$$\vec{d} = P\vec{c}. \quad (15)$$

117 With the covariance matrix $C := \langle \vec{d} \otimes \vec{d} \rangle$ of the scaled luminosity distances \vec{d} , the maximum-
 118 likelihood solution for \vec{c} is

$$\vec{c} = (P^\top C^{-1} P)^{-1} (P^\top C^{-1}) \vec{d}. \quad (16)$$

119 The uncertainties Δc_j of the coefficients and $\Delta E(a)$ of the expansion function are obtained
 120 from the Fisher matrix $F = P^\top C^{-1} P$ in the following way. First, we diagonalise the Fisher
 121 matrix by rotating it into its eigenframe with a rotation matrix R , find its eigenvalues $\sigma_i'^{-2}$
 122 and define a vector of decorrelated coefficient uncertainties $\Delta \vec{c}' = (\sigma_1', \dots, \sigma_M')$. Second, we
 123 rotate this vector back into the frame of the Chebyshev polynomials and find $\Delta \vec{c} = R^\top \Delta \vec{c}'$. The
 124 uncertainties Δc_i obtained this way are slightly larger than the Cramer-Rao bound $F_{ii}^{-1/2}$, as
 125 they are expected to be. Beginning with a large number M of coefficients, only those are kept
 126 which are statistically significant, i.e. which satisfy $|c_j| \geq \Delta c_j$.

127 2.2 Cosmic expansion function from the SN sample

128 We first reconstruct the expansion function using the Pantheon sample of type-Ia supernovae [9],
 129 covering the scale-factor range $a \in [0.3067, 1]$. This sample has been criticised by [10] for
 130 being significantly discrepant from another established type-Ia supernovae sample (the JLA
 131 sample [11]) and for methods used in the post-processing of the observed data, especially
 132 peculiar velocity corrections. We use this sample nonetheless to prove the principle. All
 133 quantitative results in this work hinge on the reliability of the data. Possible systematics in the
 134 data may be the most likely reason for some of our results deviating from Λ CDM.

135 We apply the algorithm described in the preceding subsection to derive the function $e(a)$
 136 defined in Eq. (8). Using the covariance matrix provided with the data, we determine the
 137 coefficient vector \vec{c} using Eq. (16) and derive its uncertainty $\Delta \vec{c}$ as described above. We arrive
 138 at $M = 3$ significant coefficients.

139 We then transform to $E(a)$ via Eq. (8) and determine its uncertainty from

$$\frac{\Delta E(a)}{E(a)} = \frac{\Delta e(a)}{e(a)}. \quad (17)$$

140 Our result for the expansion function and its uncertainty are shown in Fig. 1. The uncertainties
 141 are very small because the entire information taken from the SN sample is compressed into

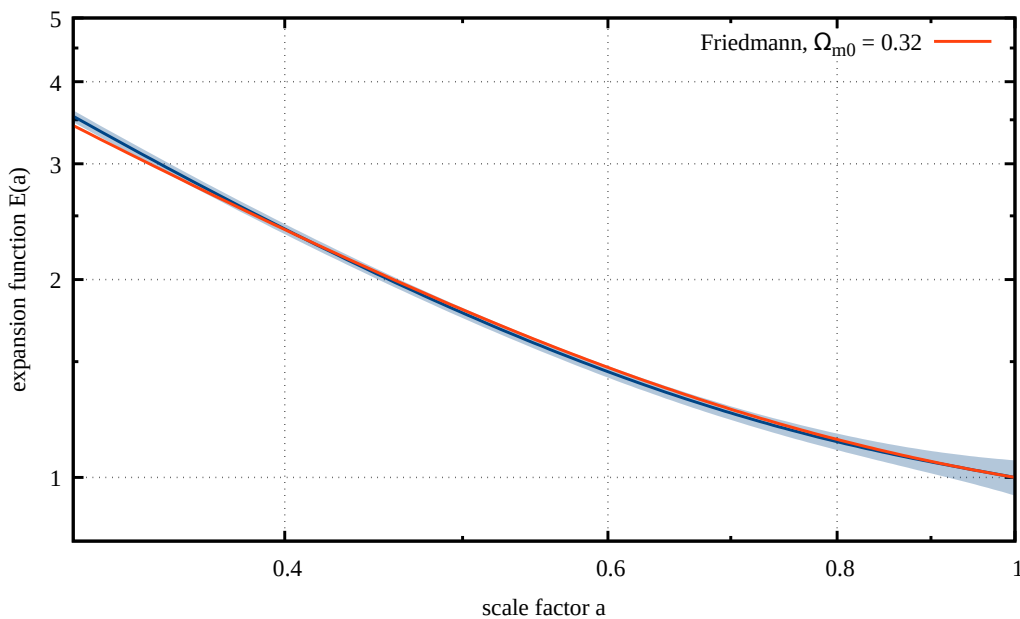


Figure 1: The cosmic expansion function $E(a)$ is shown here as reconstructed from the luminosity-distance measurements in the SN sample. Spanned by the shifted Chebyshev polynomials $T_j^*(a)$, the model needs three significant coefficients c_j whose error bars are determined by the covariance matrix of the data (see the entries in Tab. 1). The $1\text{-}\sigma$ uncertainty shown here is so small because the entire information from the data set is thus compressed into three numbers. The red line shows the best-fitting, spatially-flat, Friedmann expansion function.

142 three coefficients here. Another reason is that the uncertainties assigned to the Pantheon data
 143 are already very small compared to other SN samples. The best-fitting Λ CDM model with

$$E_{\Lambda\text{CDM}}(a) = (\Omega_{m0}a^{-3} + 1 - \Omega_{m0})^{1/2}, \quad (18)$$

144 in the common parameterisation of Eq. (1) and further assuming $\Omega_{r0} = 0$ and $\Omega_{K0} = 0$, requires
 145 $\Omega_{m0} = 0.324 \pm 0.002$. It is overplotted in red in Fig. 1.

146 2.3 Cosmic expansion function from the SN-BAO sample

147 We repeat our analysis with the combined SN-BAO sample. We collected a sample of BAO
 148 measurements by searching the reviewed literature for papers that appeared between January,
 149 2014, and December, 2018. We selected 21 papers according to the quality and the completeness
 150 of the data description and collected 89 measurements of the angular-diameter distance
 151 $D_{\text{ang}}/r_{\text{d, fid}}$ in terms of a fiducial value $r_{\text{d, fid}}$ for the so-called drag distance, setting the physical
 152 scale of the BAOs. The drag distance is the sound horizon at the end of the baryon-drag epoch.
 153 Of these measurements, we kept 75 after removing those that seemed to be either dependent
 154 on or superseded by other measurements (see Appendix C). These measurements fall into the
 155 redshift range $[0.24, 2.4]$ and thus extend the scale-factor range of our reconstruction of the
 156 expansion function.

157 The drag distance $r_{\text{d, fid}}$ is unknown to us. It is determined by

$$r_{\text{d}} = \frac{1}{H_0} \int_0^{a_{\text{d}}} \frac{c_s(a) da}{a^2 E(a)} \quad (19)$$

158 and thus needs for its theoretical calculation the expansion function for scale factors smaller than
 159 $a_{\text{d}} \approx 1100^{-1}$. In order to remain as model-independent as possible, we choose to determine r_{d}

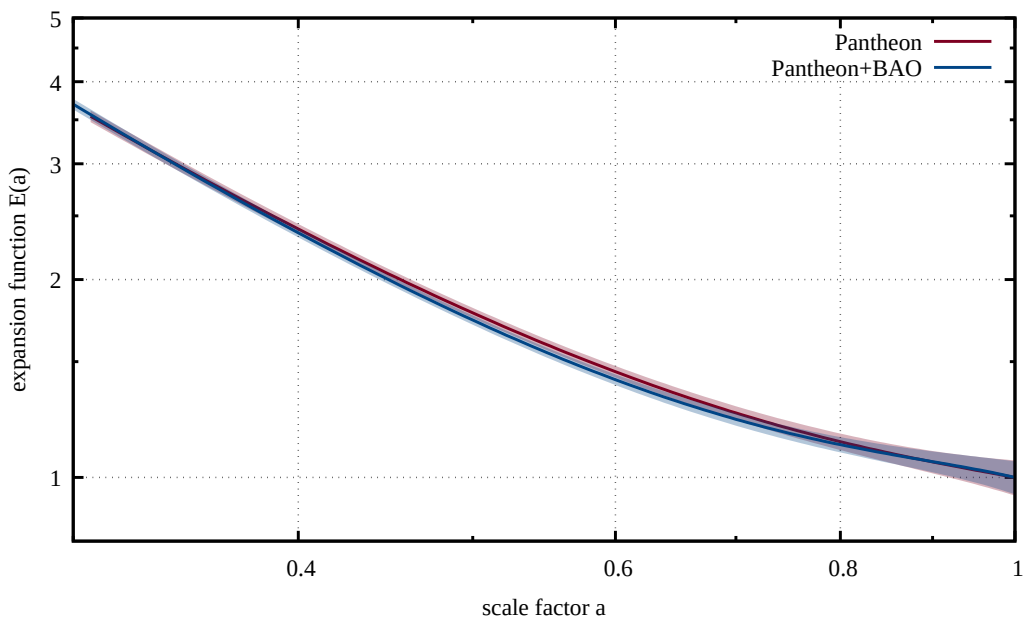


Figure 2: Expansion functions determined from the SN-BAO sample and from the SN sample alone for comparison. As in Fig. 1, $1\text{-}\sigma$ uncertainties are shown. The best-fitting, spatially-flat Friedmann expansion function is the same as in Fig. 1 and thus not repeated here. The reconstruction of $E(a)$ from the combined samples requires four significant coefficients (cf. Tab. 1).

160 by an empirical calibration: we apply an offset to the distance moduli derived from the BAO
 161 measurements such as to bring them into least-squared distance with the sample of distance
 162 moduli from the SN sample. This corresponds to cross-calibrating the drag distance to match
 163 absolute SN-Ia luminosities. This offset turns out to be redshift-independent, as expected. Its
 164 value of $\Delta\mu = 10.783 \pm 0.041$ corresponds to a drag distance of

$$r_d = 143.4 \pm 2.7 \text{ Mpc}, \quad (20)$$

165 in good agreement with the value expected in the standard Λ CDM cosmology. We further
 166 estimate the covariance matrix of the BAO data via the uncertainties quoted in the papers,
 167 combine the two statistically fully independent samples and repeat the determination of the
 168 coefficients \vec{c} and the expansion function as for the SN sample alone. The result is shown in
 169 Fig. 2. For the SN-BAO sample, we obtain $M = 4$ significant coefficients.

170 Within their uncertainties, the expansion functions obtained from the SN sample alone and
 171 from the SN-BAO sample agree with each other, but the uncertainties due to the combined
 172 sample are somewhat smaller, and the redshift range of the reconstruction is slightly extended.
 173 The fit to the standard- Λ CDM expansion function leads to a result virtually indistinguishable
 174 from the SN sample alone, with $\Omega_{m0} = 0.319 \pm 0.002$, and is therefore not shown again in
 175 Fig. 2.

176 Interestingly, the expansion function determined purely from the data is slightly more
 177 curved than the best-fitting Friedmann-Lemaître model. This difference is formally highly
 178 significant, but, as argued above, we do not want to emphasise it since it is likely to be caused
 179 by systematic biases in the data or their interpretation. The expansion coefficients determined
 180 from both data sets, i.e. from the SN sample and from the SN-BAO sample, are listed in Tab. 1.

181 Albeit likely premature in view of possible systematics in the data, it is interesting to use
 182 the reconstructed expansion function to constrain the hypothetical time evolution of the dark
 183 energy. If the expansion function $E(a)$ derived from the data were to be represented by the

Table 1: Significant expansion coefficients \vec{c} and their uncertainties $\Delta\vec{c}$.

Sample		order j			
SN sample	c_j	0.988	-0.372	0.045	
	Δc_j	0.033	0.035	0.018	
SN-BAO sample	c_j	0.983	-0.374	0.034	0.007
	Δc_j	0.029	0.032	0.017	0.001

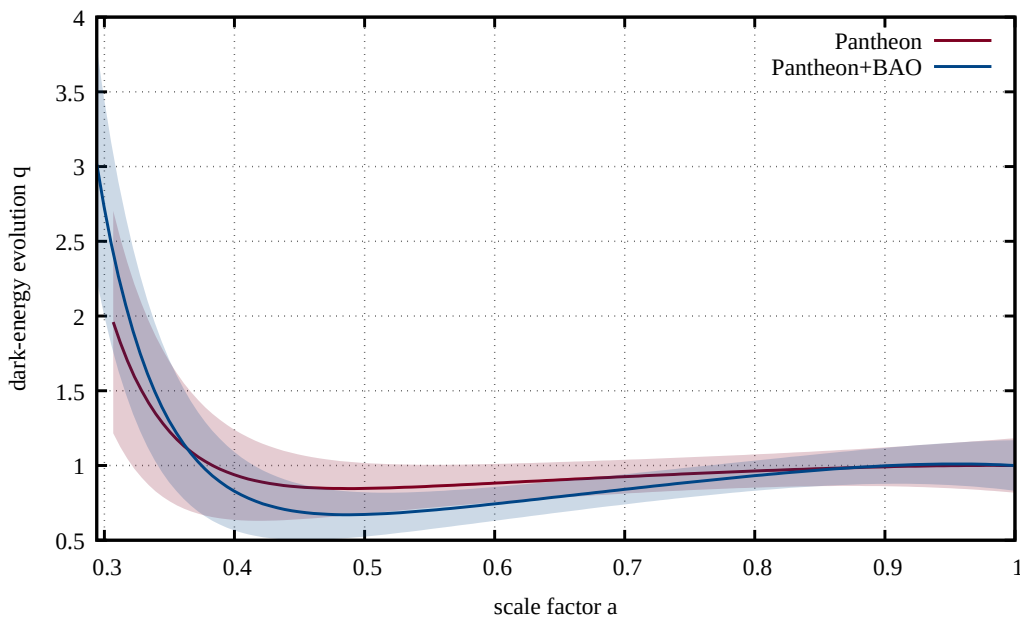


Figure 3: Constraints on a dynamical evolution of dark energy $q(a)$ as given in Eq. 22, obtained by comparing the expansion functions derived from the SN-BAO sample with the expectation for a spatially-flat Friedmann-Lemaître model (blue). The red band shows analogous constraints obtained from the SN sample only. As in Figs. 1 and 2, $1-\sigma$ uncertainties are shown.

184 expansion function $E_{\Lambda\text{CDM}}(a)$ for a spatially-flat Friedmann-Lemaître model with dynamical
 185 dark energy, we should have

$$E^2(a) \stackrel{!}{=} \Omega_{m0} a^{-3} + (1 - \Omega_{m0}) q(a), \quad (21)$$

186 which would imply

$$q(a) = \frac{E^2(a) - \Omega_{m0} a^{-3}}{1 - \Omega_{m0}}, \quad \Delta q(a) = \left| \frac{2E(a)}{1 - \Omega_{m0}} \right| \Delta E(a), \quad (22)$$

187 for the function $q(a)$ quantifying the time evolution of the dark energy and its uncertainty. This
 188 function is shown in Fig. 3 for the SN and the SN-BAO sample, setting $\Omega_{m0} = 0.32$ as obtained
 189 from the best-fitting ΛCDM model determined above. It illustrates one of the advantages of
 190 our approach, as the empirically determined expansion function does not assume any specific
 191 cosmological model in general, nor a specific model for dynamical dark energy in particular.
 192 In view of its $1-\sigma$ uncertainty show in Fig. 3, the derived function $q(a)$ does not deviate
 193 significantly from the ΛCDM result $q(a) = 1$.

194 **3 Linear growth of cosmic structures**

195 **3.1 Equation to be solved**

196 Relative to the background expanding as described by $E(a)$, structures grow under the influence
 197 of the additional gravitational field of density fluctuations $\delta\rho(\vec{x}, t) = \bar{\rho}(t)\delta(\vec{x}, t)$, where $\bar{\rho}(t)$
 198 is the mean matter density and δ the density contrast. Structures small compared to the
 199 curvature radius of the spatial sections of the universe with a density contrast $\delta \lesssim 1$ can be
 200 treated as linear perturbations of a cosmic fluid in the framework of Newtonian gravity.

201 Linearising the corresponding Euler-Poisson system of equations in the perturbations and
 202 expressing spatial positions in comoving coordinates leads to the well-known second-order,
 203 linear differential equation

$$\ddot{\delta} + 2H\dot{\delta} = 4\pi G\bar{\rho}\delta, \tag{23}$$

204 for the density contrast δ of pressure-less dust. Since none of the terms in Eq. (23) depends on
 205 spatial scales, the solutions for δ can be separated into a time dependent function $D(t)$ and a
 206 spatially dependent function $f(\vec{x})$, writing $\delta(\vec{x}, t) = D(t)f(\vec{x})$, where $D(t)$ alone has to satisfy
 207 Eq. (23). Of the two linearly independent solutions of Eq. (23), one decreases with time and is
 208 thus irrelevant for our purposes. We focus on the growing solution $D_+(t)$, i.e. the linear growth
 209 factor. Transforming the independent variable in Eq. (23) from the time t to the scale factor a
 210 results in the equation

$$D_+'' + \left(\frac{3}{a} + \frac{E'(a)}{E(a)}\right)D_+' = \frac{3}{2} \frac{\Omega_m}{a^2} D_+, \tag{24}$$

211 for the linear growth factor, with primes denoting derivatives with respect to a . The time-
 212 dependent matter-density parameter $\Omega_m(a)$ is given by

$$\Omega_m(a) = \frac{\Omega_{m0}}{E^2(a)a^3}, \tag{25}$$

213 in terms of the expansion function $E(a)$ and the present-day matter-density parameter Ω_{m0} .
 214 Equation (24) thus depends only on the expansion function $E(a)$, its first derivative, and the
 215 present matter-density parameter Ω_{m0} . We know $E(a)$ empirically in a model-independent way
 216 from the procedure described in Sect. 2.

217 **3.2 Initial conditions and results for the linear growth factor**

218 Before we can proceed to solve Eq. (24) for the growth factor, we need to set Ω_{m0} and to specify
 219 initial conditions. Since we know $E(a)$ from data taken in the scale-factor interval $[a_{\min}, 1]$, we
 220 need to set the initial conditions at a_{\min} . Since Eq. (24) is homogeneous, the initial value of D_+
 221 is irrelevant and can be set to any arbitrary value. We choose $D_+(a_{\min}) = 1$. Concerning the
 222 derivative $D_+'(a)$ at $a = a_{\min}$, we begin with the *ansatz* $D_+ = a^n$ near $a = a_{\min}$, assume that n
 223 changes only slowly with a and use Eq. (24) to find

$$n = \frac{1}{4} \left[-1 - \varepsilon + \sqrt{(1 + \varepsilon)^2 + 24(1 - \omega)} \right], \tag{26}$$

224 for the growing solution, using the definitions

$$\varepsilon := 3 + 2 \frac{d \ln E}{d \ln a} \quad \text{and} \quad \omega := 1 - \Omega_m(a). \tag{27}$$

225 In the matter-dominated phase, both ε and ω are small compared to unity, and n is approxi-
 226 mately

$$n \approx 1 - \frac{\varepsilon + 3\omega}{5}. \tag{28}$$

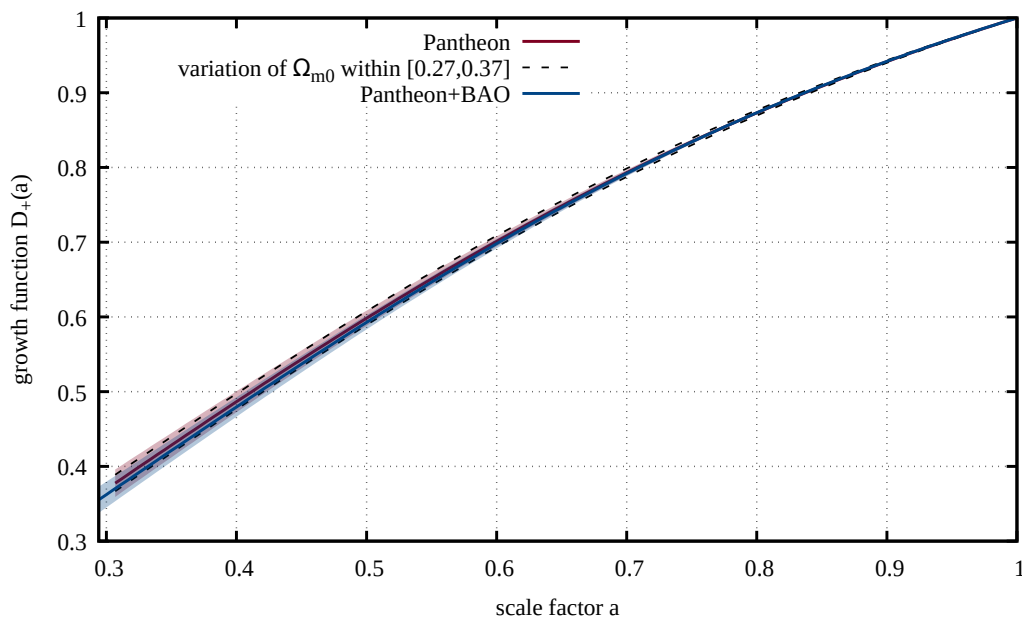


Figure 4: Linear growth factors $D_+(a)$ implied by the two expansion functions $E(a)$ shown in Fig. 2, obtained from the SN-BAO sample (blue) and from the SN sample alone (red). As described in the text, the growth factors are obtained by solving Eq. (25) using the empirically derived expansion functions and setting Ω_{m0} to the value implied by the best-fitting Λ CDM model. The shaded areas cover the $1-\sigma$ uncertainty propagated from the uncertainty of the expansion function $E(a)$. This uncertainty is comparable to the effect of varying Ω_{m0} within $[0.27, 0.37]$ which is indicated by dashed lines in the example of the SN sample.

227 With the reconstructed expansion rate $E(a)$, the parameter ε is fixed. For any choice of Ω_{m0} ,
 228 also ω is set via Eq. (25), thus so is the growth exponent n , and we can start integrating the
 229 growth function with the remaining initial condition

$$D'_+(a_{\min}) = na_{\min}^{n-1} = \frac{nD_+(a_{\min})}{a_{\min}} = \frac{n}{a_{\min}}. \quad (29)$$

230 For each choice of Ω_{m0} , we can now solve Eq. (24) with the initial conditions Eq. (29) and
 231 $D_+(a_{\min}) = 1$. Having arrived at $a = 1$, we normalise the growth factor such that it is unity
 232 today, $D_+(a = 1) = 1$. The uncertainty of the expansion function $E(a)$ propagates to $D_+(a)$,
 233 but the uncertainty on D_+ shrinks towards $a = 1$ because of this normalisation. The result is
 234 shown in Fig. 4 for Ω_{m0} as derived from the fit to the expansion function.

235 The uncertainties from both the growth exponent n and the fitted matter-density parameter
 236 Ω_{m0} , disappear in the line width of the plot. The shaded areas in Fig. 4 correspond to the
 237 propagated $1-\sigma$ uncertainties of the coefficients \tilde{c} defining the expansion function and are
 238 calculated as explained in [12]. These uncertainties are comparable to the effect of varying
 239 Ω_{m0} in the range $[\Omega_{m0} - 0.05, \Omega_{m0} + 0.05]$ as indicated by the dashed lines in the same figure.
 240 Hence, the growth function depends only weakly on reasonably sized variations of Ω_{m0} .

241 3.3 The growth index of linear perturbations

242 A common representation of the derivative of the growth factor with respect to the scale factor
 243 is given by the growth index γ , defined by

$$\frac{d \ln D_+}{d \ln a} =: f(\Omega_m) = \Omega_m^{\gamma(a)}. \quad (30)$$

244 Theoretically predicted values of γ that can be found in the literature [13–20] range from
 245 approximately $\gamma = 0.4$ (for some $f(R)$ modifications of gravity [21]) to $\gamma = 0.7$. This range
 246 includes models with varying dark-energy equation of state [13, 19], curved-space models [18]
 247 and models beyond general relativity [13, 14, 21, 22]. Even for models with strongly varying γ ,
 248 the values for redshifts $z \in [0, 2]$ are usually very close to $\gamma \sim 0.6$.

249 Without further specification, Eq. (30) is obviously valid for any cosmology since the
 250 growth index $\gamma(a)$ could be any function of a . An advantage of writing the logarithmic slope
 251 of the growth function in this way is that $\gamma(a)$ is very well constrained for a wide range of
 252 cosmological models and can be used as a diagnostic for the classification of models based
 253 on gravity theories even beyond general relativity [13, 14]. For a recent and well structured
 254 review about constraints for γ in a wide range of models, see [14].

255 Another substantial advantage of Eq. (30) is that γ happens to be almost constant within a
 256 wide range of models. [15] found a general expression for $\gamma(a)$ that applies to any model with
 257 a mixture of cold dark matter plus cosmological constant (Λ CDM) or quintessence (QCDM).
 258 For example, for a dark-energy equation of state parameterised by a slowly varying function
 259 $w(\Omega_m)$ in a spatially-flat universe, the growth index reduces to

$$\gamma = \frac{3(w-1)}{6w-5} \quad (31)$$

260 [16]. Thus, for any constant w , the growth index γ is itself constant and reduces to
 261 $\gamma = 6/11 \approx 0.55$ for Λ CDM.

262 It is interesting in our context that we can derive γ based on the reconstructed expansion
 263 function $E(a)$. As we show in Appendix B, an approximate, yet sufficiently accurate solution
 264 for γ is

$$\gamma = \frac{\varepsilon + 3\omega}{2\varepsilon + 5\omega}. \quad (32)$$

265 For a Λ CDM model,

$$\frac{2aE'}{E} = \frac{2a}{E} \left(\frac{-3\Omega_{m0}a^{-4}}{2E} \right) = -3 \frac{\Omega_{m0}}{E^2 a^3} = -3(1-\omega), \quad (33)$$

266 thus $\varepsilon = 3\omega$ from Eq. (27), and Eq. (32) reduces to $\gamma = 6/11$. With our reconstruction of the
 267 expansion function E , we can determine γ and its uncertainty

$$\Delta\gamma = \left[\left(\frac{\partial\gamma}{\partial c_j} \right)^2 \Delta c_j^2 \right]^{1/2}, \quad (34)$$

268 for any choice of Ω_{m0} . The result for Ω_{m0} as derived from the fit to the expansion function is
 269 shown for both data samples in Fig. 5.

270 The growth index follows the Λ CDM result very closely for $a \gtrsim 0.45$, but increases for
 271 smaller scale factors. Furthermore, its uncertainty for the combined SN-BAO sample is larger
 272 than for the SN sample alone. This indicates that the two data sets are not fully compatible. It
 273 is thus likely that systematic errors in the data or any unaccounted covariance between the
 274 data points is responsible for the behaviour of γ at $a \lesssim 0.45$. We will further comment on these
 275 deviations from the Λ CDM expectation in Sec. 4. Here, we conclude by pointing out that our
 276 reconstruction method allows a direct determination of the growth index γ .

277 4 Comparison of different data samples

278 While our method is model-independent in the sense discussed above, existing SN and BAO
 279 samples may depend on several model assumptions because they consist of measurements that

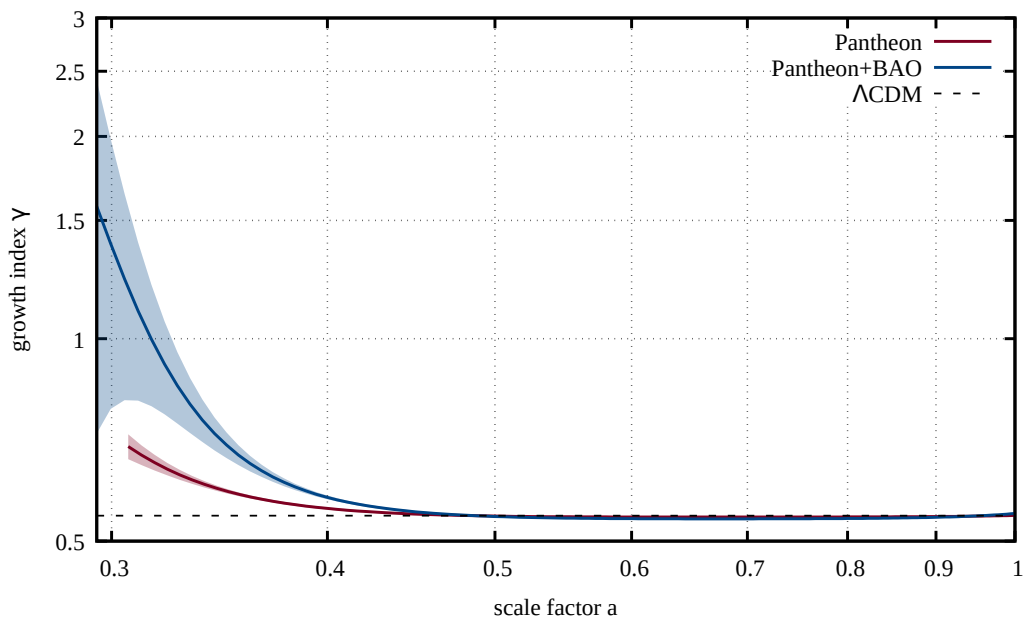


Figure 5: Growth index γ derived from the expansion function E , reconstructed from the SN sample and from the SN-BAO sample, adopting $\Omega_{m0} = 0.319$. The fact that the uncertainty increases for the combined data sets at $a \lesssim 0.4$ indicates that the individual data sets are not fully compatible.

280 have been post-processed in sequences of non-trivial steps. Some of these steps may sensitively
 281 depend on cosmological model assumptions. Hence, while our algorithm itself makes no
 282 reference to a specific cosmological model, the functions we derive with it may reflect intrinsic
 283 model-dependences as well as biases possibly introduced into the data in the reduction process.
 284 In fact, existing data samples are partly incompatible with each other, and some post-processing
 285 steps are controversially discussed in the literature (e.g. [10]).

286 To give the reader an idea of how the differences between currently available SN and BAO
 287 samples affect the results obtained by our model-independent approach, we repeat the whole
 288 analysis with a second sample of type-Ia SNe (the Union-2.1 sample, [23]) alone, and with this
 289 sample combined with the BAO sample. We thus contrast results obtained from four samples,
 290 i.e. the Pantheon sample, the Union-2.1 sample, and the two combined samples Pantheon+BAO
 291 and Union-2.1+BAO.

292 The four functions discussed in this paper, i.e. the expansion function $E(a)$, the dark-energy
 293 evolution $q(a)$, the growth function $D_+(a)$, and the growth index $\gamma(a)$, are plotted for the four
 294 data samples in Fig. 6. This comparison is meant to illustrate variations between samples but
 295 does not allow any quantitative conclusions about the quality of individual data sets, especially
 296 since both SN samples (as well as other established samples like the JLA sample) share large
 297 amounts of raw data as well as essential post-processing tools.

298 The top left panel shows that the four reconstructed expansion functions are all compatible
 299 with each other in view of their uncertainties. The growth function reconstructed from the
 300 Union-2.1 sample alone is flatter than obtained from the other samples, but the three growth
 301 functions derived from the Pantheon sample alone and from the two SN+BAO samples are
 302 virtually identical. Within their $1\text{-}\sigma$ uncertainty bounds the dark energy evolution functions
 303 $q(a)$ reconstructed from the four samples are partly not compatible with each other and with
 304 $q(a) = 1$. For scale factors $a \lesssim 0.4$, the functions derived from the Pantheon sample and the
 305 two samples combined with BAO data turn upward, but in view of their $3\text{-}\sigma$ uncertainty bounds
 306 this tendency is so far not significant.

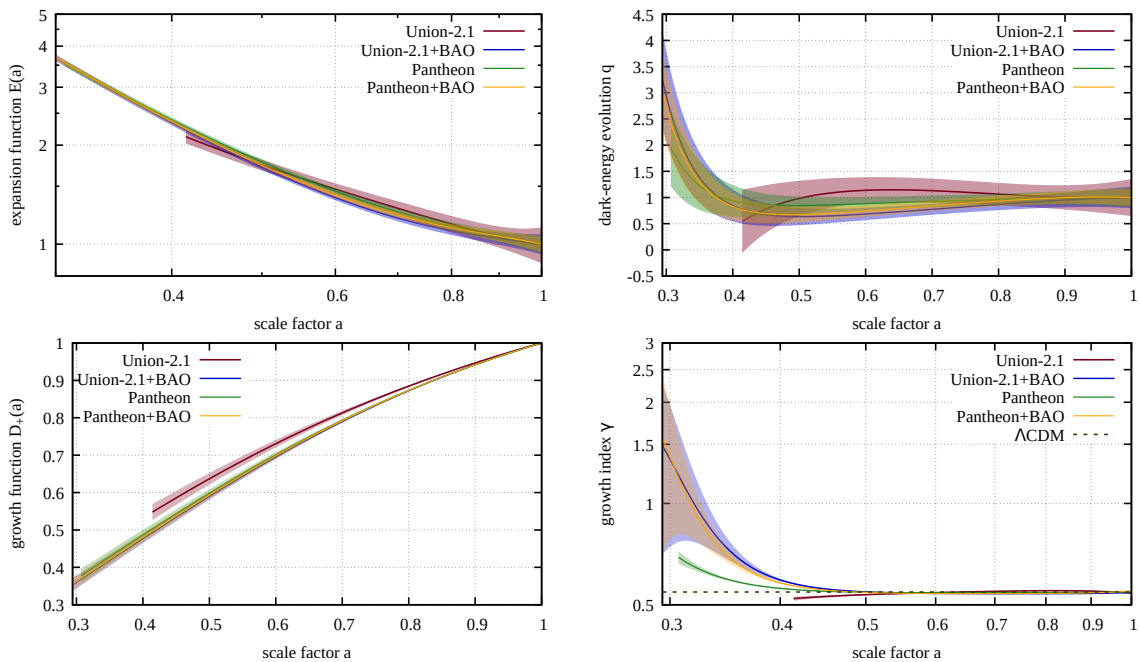


Figure 6: Each panel shows results obtained from four data samples: the Union-2.1 and Pantheon SN samples (red and green, respectively), and these two samples combined with BAOs (blue and yellow, respectively). From left to right and from top to bottom, the four panels show (a) the expansion function $E(a)$, (b) the evolution of the dark energy $q(a)$, (c) the linear growth factor $D_+(a)$, and (d) the growth index $\gamma(a)$. The growth functions obtained from the two combined SN+BAO samples are nearly indistinguishable, hence the blue line in the lower left panel is hidden behind the yellow line.

307 The growth index $\gamma(a)$ shows the largest variation across different samples. While it closely
 308 follows the Λ CDM expectation for all samples at scale factors $a \gtrsim 0.45$, the Pantheon and in
 309 particular that BAO data drive it to larger values for scale factors $a \lesssim 0.45$. Adding BAO data
 310 increases the uncertainty substantially, which indicates that the SN and BAO samples are to
 311 some degree incompatible with each other. Our cross-calibration of the BAO drag distance
 312 with the SNe only ensures that the BAO sample continuously extends the SN samples. This
 313 indication of partly incompatible data, and the enhanced uncertainty of the growth indices
 314 derived from the combined BAO and SN samples, leads us to the conclusion that we cannot
 315 take the apparent deviation from Λ CDM seriously yet. It might be an indication of systematics
 316 in the analyzed samples that would affect any cosmological analysis based on model fitting
 317 approaches.

318 Even though our method could in principle be insufficiently flexible by its restriction to
 319 the few significant Chebyshev coefficients, the expansion functions shown in Figs. 1 and 2
 320 are rather more than less curved than the best-fitting expansion function for a spatially flat,
 321 conventional Friedmann cosmology.

322 We draw three main conclusions from this analysis: first, the expansion and growth functions
 323 recovered from the largest and combined samples show only little variation in view of their
 324 uncertainties; second, the empirical calibration of the drag distance is quite insensitive to
 325 differences in the SN samples and the BAO sample stabilises the results of the combined
 326 samples; and third, the variations in the growth index and its uncertainty being larger in the
 327 combined SN+BAO samples indicate that the BAO and SN data sets are not fully compatible
 328 yet.

329 5 Conclusions

330 We have shown here how the linear growth factor $D_+(a)$ of cosmic structures can be inferred
331 from existing data with remarkably small uncertainty without reference to a specific cosmo-
332 logical model. Following up on, modifying and extending earlier studies, we have derived the
333 cosmic expansion function $E(a)$ in a way independent of the cosmological model from the
334 measurements of distance moduli to the type-Ia supernovae of the Pantheon sample and the
335 Union-2.1 sample, as well as from each of the two samples combined with a sample of BAO
336 distance measurements compiled from the literature. All we need to assume is that underlying
337 the cosmological model is a metric theory of gravity and that our universe satisfies the sym-
338 metry assumptions of spatial homogeneity and isotropy reasonably well. The uncertainty on
339 this empirically determined expansion function already is remarkably small, and the results
340 obtained from the Pantheon SN sample alone and from two SN samples combined with the
341 BAO sample agree very well with each other.

342 The expansion function obtained this way is the main ingredient for the differential Eq. (24)
343 describing cosmic structure growth in the linear limit. Only one parameter is needed to solve this
344 equation, viz. the present-day matter-density parameter Ω_{m0} , because it enters into the initial
345 conditions for solving Eq. (24) and into the equation itself. Adopting a value for Ω_{m0} derived
346 from fitting a spatially flat Friedmann model to our reconstructed expansion function, we can
347 also solve for the growth index γ defined in Eq. (30). This implies that, due to measurements
348 of the distance moduli to the type-Ia supernovae in the SN and SN-BAO samples, the expansion
349 function is accurately determined, and the linear growth factor D_+ is tightly constrained up to
350 a single remaining parameter, i.e. the present-day matter density parameter Ω_{m0} .

351 Variations of the results mainly for the growth index $\gamma(a)$ with different data samples indicate
352 that the data may contain systematic effects that may arise in the process of data reduction
353 of the SN samples that could partly be caused by implicit cosmological model assumptions.
354 Uncertainties in the growth index increasing in the combined SN+BAO samples show that the
355 different data types do not seem to be fully compatible.

356 Notwithstanding their uncertainties, our results for the dark-energy evolution $q(a)$ shown in
357 Fig. 3, and for the growth index $\gamma(a)$, shown in Fig. 5, illustrate how our method can be used
358 with future data to derive these two functions directly from distance measurements.

359 Some of our results, in particular the growth index and the time-dependence of the dark-
360 energy density, deviate from the Λ CDM expectations. In the case of the dark-energy evolution
361 function $q(a)$, these deviations are not significant. In the case of the growth index $\gamma(a)$, the
362 most likely reasons are systematic effects in the data and partial incompatibilities between data
363 samples, as discussed. We thus abstain from claiming any evidence for non-standard behaviour
364 of these functions. However, the possible presence of systematics in the data samples would be
365 a matter of concern for cosmological analyses based on Λ CDM fitting approaches, especially in
366 view of the current dispute on the value of H_0 .

367 In future work, we will extend the method presented here to further types of data. Our
368 goal is to determine the two centrally important functions of cosmology, $E(a)$ and $D_+(a)$,
369 with as few assumptions as possible and without reference to a specific cosmological model.
370 Such applications of our results may be particularly interesting which so far require assuming
371 cosmological parameters or models for a possible evolution of dark energy, e.g. cosmological
372 weak gravitational lensing.

373 **Acknowledgements**

374 It is a pleasure to thank Bettina Heinlein, Sven Meyer, Jiahan Shi, Lorenzo Speri, and Jenny
 375 Wagner for interesting and helpful discussions. This work was supported by the Deutsche
 376 Forschungsgemeinschaft (DFG) via the Transregional Collaborative Research Centre TRR 33
 377 (MB, MM) and under Germany's Excellence Strategy EXC-2181/1 - 390900948 (the Heidelberg
 378 STRUCTURES Excellence Cluster).

379 **A Chebyshev polynomials**

380 The (unnormalised) Chebyshev polynomials of the first kind $\bar{T}_n(x)$ are defined on the interval
 381 $[-1, 1]$ by the recurrence relation

$$\bar{T}_{n+1}(x) = 2x\bar{T}_n(x) - \bar{T}_{n-1}(x), \tag{A.1}$$

382 with $\bar{T}_0(x) = 1$ and $\bar{T}_1(x) = x$. They can be written in the form

$$\bar{T}_n(\cos \theta) = \cos n\theta \tag{A.2}$$

383 and are orthogonal (but not orthonormal) with respect to the weight function
 384 $w(x) = (1 - x^2)^{-1/2}$,

$$\begin{aligned} \langle \bar{T}_n(x)\bar{T}_m(x) \rangle &= \int_{-1}^1 \frac{dx}{\sqrt{1-x^2}} \bar{T}_n(x)\bar{T}_m(x) = \int_0^\pi d\theta \cos n\theta \cos m\theta \\ &= \begin{cases} 0 & n \neq m \\ \pi & n = m = 0 \\ \pi/2 & n = m \neq 0 \end{cases}. \end{aligned} \tag{A.3}$$

385 The normalised Chebyshev polynomials are thus given by

$$T_n(x) := \begin{cases} (1/\pi)^{1/2} & (n = 0) \\ (2/\pi)^{1/2} \cos(n \arccos x) & (n > 0) \end{cases}. \tag{A.4}$$

386 Finally, the shifted Chebyshev polynomials are defined on the interval $[0, 1]$ in terms of the
 387 Chebyshev polynomials by

$$T_n^*(x) = T_n(2x - 1). \tag{A.5}$$

388 They are orthonormal with respect to the weight function $w^*(x) = (x - x^2)^{-1/2}$.

389 **B Derivation of the growth index**

390 In terms of the logarithmic derivative

$$f := \frac{d \ln D_+}{d \ln a} \tag{B.1}$$

391 and using the parameters ε and ω introduced in Eq. (27), the linear growth equation (24)
 392 reads

$$\frac{df}{d \ln a} + \frac{1}{2}(1 + \varepsilon)f + f^2 = \frac{3}{2}(1 - \omega). \tag{B.2}$$

393 We write

$$\frac{df}{d \ln a} = f \frac{d \ln \Omega_m}{d \ln a} \frac{d \ln f}{d \ln \Omega_m}, \quad (\text{B.3})$$

394 use Eq. (25) to find

$$\frac{d \ln \Omega_m}{d \ln a} = -\varepsilon \quad (\text{B.4})$$

395 and Eq. (30) to write

$$\frac{d \ln f}{d \ln \Omega_m} = \gamma - \omega \frac{d \gamma}{d \ln \Omega_m}, \quad (\text{B.5})$$

396 approximating $\ln \Omega_m = \ln(1 - \omega) \approx -\omega$ in the last step. Neglecting terms of order $\varepsilon \omega$, we have

$$\frac{df}{d \ln a} = -\varepsilon \gamma f. \quad (\text{B.6})$$

397 Inserting this result into Eq. (B.2), dividing by f and approximating

$$f = \Omega_m^\gamma = (1 - \omega)^\gamma \approx 1 - \gamma \omega, \quad (\text{B.7})$$

398 we arrive at

$$-\varepsilon \gamma + \frac{1}{2}(1 + \varepsilon) + 1 - \gamma \omega = \frac{3}{2}[1 + (\gamma - 1)\omega], \quad (\text{B.8})$$

399 to linear order in ε and ω . Solving for γ finally gives the result

$$\gamma = \frac{\varepsilon + 3\omega}{2\varepsilon + 5\omega}, \quad (\text{B.9})$$

400 quoted in Eq. (32).

401 C BAO sample

402 The sample of BAO measurements collected from the literature is listed in Tab. 2.

Table 2: BAO data.

n	z	D_A/r_d	$\Delta(D_A/r_d)$	Description	Reference
1	0.240	5.3637	0.4673	autocorrelation function of CMASS galaxies in BOSS DR12	[24]
2	0.240	5.5939	0.3048	redshift-space distortion moments of LOWZ and CMASS galaxy samples in BOSS DR12	[25]
3	0.310	6.2900	0.1400	tomographic configuration-space analysis of galaxy autocorrelations in BOSS DR12	[26]
4	0.310	6.2948	0.1963	tomographic analysis of galaxy clustering in BOSS DR12	[27]
5	0.310	6.3045	0.2734	tomographic analysis of redshift-space distortion moments in BOSS DR12 galaxies	[28]
6	0.320	6.6978	0.2099	autocorrelation function of CMASS galaxies in BOSS DR12	[24]
7	0.320	6.4743	0.1896	redshift-space distortion moments of LOWZ and CMASS galaxy samples in BOSS DR12	[25]
8	0.320	6.6689	0.3943	autocorrelation function of CMASS and LOWZ galaxies in BOSS DR12, $z = 0.3-0.5$	[29]
9	0.320	6.6600	0.1600	analysis of redshift-space distortion moments in BOSS DR14 quasars	[30]
10	0.360	7.0900	0.1600	tomographic configuration-space analysis of galaxy autocorrelations in BOSS DR12	[26]
11	0.360	6.9379	0.2572	tomographic analysis of galaxy clustering in BOSS DR12	[27]
12	0.360	7.0870	0.2390	tomographic analysis of redshift-space distortion moments in BOSS DR12 galaxies	[28]
13	0.370	7.3818	0.3318	autocorrelation function of CMASS galaxies in BOSS DR12	[24]
14	0.370	6.7249	0.4402	redshift-space distortion moments of LOWZ and CMASS galaxy samples in BOSS DR12	[25]
15	0.380	7.4435	0.2730	galaxy clustering in BOSS DR12, combined with various priors	[31]
16	0.380	7.3894	0.1218	power spectrum of galaxy distribution in BOSS DR12	[32]
17	0.380	7.3894	0.1116	galaxy clustering in BOSS DR12, systematic-error analysis	[33]
18	0.400	7.7000	0.1600	tomographic configuration-space analysis of galaxy autocorrelations in BOSS DR12	[26]
19	0.400	7.5335	0.2166	tomographic analysis of galaxy clustering in BOSS DR12	[27]
20	0.400	7.6576	0.2407	tomographic analysis of redshift-space distortion moments in BOSS DR12 galaxies	[28]
21	0.440	8.2000	0.1300	tomographic configuration-space analysis of galaxy autocorrelations in BOSS DR12	[26]
22	0.440	8.0547	0.1760	tomographic analysis of galaxy clustering in BOSS DR12	[27]

Table 2: BAO data (continued).

n	z	D_A/r_d	$\Delta(D_A/r_d)$	Description	Reference
23	0.440	8.0464	0.1601	tomographic analysis of redshift-space distortion moments in BOSS DR12 galaxies	[28]
24	0.450	8.2881	0.2954	angular galaxy clustering in SDSS DR10	[34]
25	0.470	7.7682	0.3869	angular galaxy clustering in SDSS DR10	[34]
26	0.480	8.6400	0.1100	tomographic configuration-space analysis of galaxy autocorrelations in BOSS DR12	[26]
27	0.480	8.6977	0.1895	tomographic analysis of galaxy clustering in BOSS DR12	[27]
28	0.480	8.6059	0.1812	tomographic analysis of redshift-space distortion moments in BOSS DR12 galaxies	[28]
29	0.490	7.7100	0.3245	angular galaxy clustering in SDSS DR10	[34]
30	0.490	8.7092	0.2641	autocorrelation function of CMASS galaxies in BOSS DR12	[24]
31	0.490	8.7227	0.2099	redshift-space distortion moments of LOWZ and CMASS galaxy samples in BOSS DR12	[25]
32	0.510	7.8926	0.2789	angular galaxy clustering in SDSS DR10	[34]
33	0.510	8.8510	0.1264	galaxy clustering in BOSS DR12, systematic-error analysis	[33]
34	0.520	8.9000	0.1200	tomographic configuration-space analysis of galaxy autocorrelations in BOSS DR12	[26]
35	0.520	9.0565	0.2031	tomographic analysis of galaxy clustering in BOSS DR12	[27]
36	0.520	9.0465	0.1984	tomographic analysis of redshift-space distortion moments in BOSS DR12 galaxies	[28]
37	0.530	8.7336	0.6107	angular galaxy clustering in SDSS DR10	[34]
38	0.550	8.7021	0.5119	angular galaxy clustering in SDSS DR10	[34]
39	0.560	9.1600	0.1400	tomographic configuration-space analysis of galaxy autocorrelations in BOSS DR12	[26]
40	0.560	9.3813	0.2031	tomographic analysis of galaxy clustering in BOSS DR12	[27]
41	0.560	9.3778	0.2077	tomographic analysis of redshift-space distortion moments in BOSS DR12 galaxies	[28]
42	0.570	9.5241	0.1428	autocorrelation function of CMASS and LOWZ galaxies in BOSS DR12, $z = 0.3-0.5$	[29]
43	0.570	9.4200	0.1300	analysis of redshift-space distortion moments in BOSS DR14 quasars	[30]
44	0.590	9.5896	0.1693	autocorrelation function of CMASS galaxies in BOSS DR12	[24]
45	0.590	9.6235	0.1558	redshift-space distortion moments of LOWZ and CMASS galaxy samples in BOSS DR12	[25]
46	0.590	9.4500	0.1700	tomographic configuration-space analysis of galaxy autocorrelations in BOSS DR12	[26]
47	0.590	9.5167	0.2301	tomographic analysis of galaxy clustering in BOSS DR12	[27]
48	0.590	9.6347	0.2279	tomographic analysis of redshift-space distortion moments in BOSS DR12 galaxies	[28]

Table 2: BAO data (continued).

n	z	D_A/r_d	$\Delta(D_A/r_d)$	Description	Reference
49	0.610	9.6292	0.1593	galaxy clustering in BOSS DR12, systematic-error analysis	[33]
50	0.640	9.9011	0.2844	autocorrelation function of CMASS galaxies in BOSS DR12	[24]
51	0.640	9.7792	0.2777	redshift-space distortion moments of LOWZ and CMASS galaxy samples in BOSS DR12	[25]
52	0.640	9.6200	0.2200	tomographic configuration-space analysis of galaxy autocorrelations in BOSS DR12	[26]
53	0.640	9.5573	0.2775	tomographic analysis of galaxy clustering in BOSS DR12	[27]
54	0.640	9.8065	0.3849	tomographic analysis of redshift-space distortion moments in BOSS DR12 galaxies	[28]
55	0.800	10.3720	0.9699	Fourier-space measurement of clustering of eBOSS DR14 quasars	[35]
56	0.800	10.8119	1.1428	clustering of 147000 eBOSS DR14 quasars	[36]
57	0.978	10.7334	1.9281	tomographic analysis of quasar clustering in eBOSS DR14	[37]
58	1.000	12.0449	0.9880	Fourier-space measurement of clustering of eBOSS DR14 quasars	[35]
59	1.000	11.5205	1.0319	clustering of 147000 eBOSS DR14 quasars	[36]
60	1.230	11.9710	1.0805	tomographic analysis of quasar clustering in eBOSS DR14	[37]
61	1.500	12.0693	0.7443	Fourier-space measurement of clustering of eBOSS DR14 quasars	[35]
62	1.500	12.1559	0.7362	clustering of 147000 eBOSS DR14 quasars	[36]
63	1.520	12.5186	0.7443	combination of power spectrum and bispectrum of BOSS DR12 galaxies	[38]
64	1.520	12.5186	0.6767	clustering of 148659 quasars from eBOSS DR14 survey	[39]
65	1.526	11.9689	0.6536	tomographic analysis of quasar clustering in eBOSS DR14	[37]
66	1.944	12.2343	0.9911	tomographic analysis of quasar clustering in eBOSS DR14	[37]
67	2.000	12.3585	0.5391	Fourier-space measurement of clustering of eBOSS DR14 quasars	[35]
68	2.000	12.0111	0.5616	clustering of 147000 eBOSS DR14 quasars	[36]
69	2.200	12.1697	0.4969	Fourier-space measurement of clustering of eBOSS DR14 quasars	[35]
70	2.200	11.8546	0.5392	clustering of 147000 eBOSS DR14 quasars	[36]
71	2.225	10.0425	1.7588	autocorrelation function of BOSS DR12 quasars	[40]
72	2.330	11.3423	0.6396	Lya forest in 157783 BOSS DR12 quasars	[41]
73	2.340	11.2754	0.6513	Lya forest in 137562 BOSS DR11 quasars	[42]
74	2.360	10.8000	0.4000	Lya forest in 137562 BOSS DR11 quasars	[42]
75	2.400	10.5000	1.2513	cross-correlation between 234367 quasars and 168889 forests in BOSS	[43]

403 **References**

- 404 [1] A. G. Riess et al., *Observational evidence from supernovae for an accelerating universe and*
405 *a cosmological constant*, *Astron. J.* **116**, 1009 (1998), doi:[10.1086/300499](https://doi.org/10.1086/300499).
- 406 [2] S. Perlmutter et al., *Measurements of Ω and Λ from 42 high-redshift supernovae*, *ApJ* **517**,
407 565 (1999), doi:[10.1086/307221](https://doi.org/10.1086/307221).
- 408 [3] M. S. Turner and M. White, *CDM models with a smooth component*, *Phys. Rev. D* **56**, R4439
409 (1997), doi:[10.1103/PhysRevD.56.R4439](https://doi.org/10.1103/PhysRevD.56.R4439).
- 410 [4] C. Mignone and M. Bartelmann, *Model-independent determination of the cosmic expansion*
411 *rate*, *A&A* **481**, 295 (2008), doi:[10.1051/0004-6361:20078983](https://doi.org/10.1051/0004-6361:20078983).
- 412 [5] M. Maturi and C. Mignone, *An optimal basis system for cosmology: Data analysis and new*
413 *parameterisation*, *A&A* **508**, 45 (2009), doi:[10.1051/0004-6361/200912451](https://doi.org/10.1051/0004-6361/200912451).
- 414 [6] P. A. R. Ade et al., *Planck 2015 results. XIII. Cosmological parameters*, *A&A* **594**, A13
415 (2016), doi:[10.1051/0004-6361/201525830](https://doi.org/10.1051/0004-6361/201525830).
- 416 [7] N. Suzuki et al., *The Hubble space telescope cluster supernova survey. V. Improving the*
417 *dark-energy constraints above $z > 1$ and building an early-type-hosted supernova sample*,
418 *ApJ* **746**, 85 (2012), doi:[10.1088/0004-637X/746/1/85](https://doi.org/10.1088/0004-637X/746/1/85).
- 419 [8] S. Benitez-Herrera, E. E. O. Ishida, M. Maturi, W. Hillebrandt, M. Bartelmann and F. Röpke,
420 *Cosmological parameter estimation from SN Ia data: a model-independent approach*, *Mon.*
421 *Not. R. Astron. Soc.* **436**, 854 (2013), doi:[10.1093/mnras/stt1620](https://doi.org/10.1093/mnras/stt1620).
- 422 [9] D. M. Scolnic et al., *The complete light-curve sample of spectroscopically confirmed SNe Ia*
423 *from Pan-STARRS1 and cosmological constraints from the combined pantheon sample*, *ApJ*
424 **859**, 101 (2018), doi:[10.3847/1538-4357/aab9bb](https://doi.org/10.3847/1538-4357/aab9bb).
- 425 [10] M. Rameez and S. Sarkar, *Is there really a Hubble tension?*, *Class. Quantum Grav.* **38**,
426 154005 (2021), doi:[10.1088/1361-6382/ac0f39](https://doi.org/10.1088/1361-6382/ac0f39).
- 427 [11] M. Betoule et al., *Improved cosmological constraints from a joint analysis of the SDSS-II and*
428 *SNLS supernova samples*, *A&A* **568**, A22 (2014), doi:[10.1051/0004-6361/201423413](https://doi.org/10.1051/0004-6361/201423413).
- 429 [12] C. F. Schmidt and M. Bartelmann, *On the sensitivity of weak gravitational lensing to the*
430 *cosmic expansion function* (2020), [arXiv:2011.03202](https://arxiv.org/abs/2011.03202).
- 431 [13] E. V. Linder and R. N. Cahn, *Parameterized beyond-Einstein growth*, *Astropart. Phys.* **28**,
432 481 (2007), doi:[10.1016/j.astropartphys.2007.09.003](https://doi.org/10.1016/j.astropartphys.2007.09.003).
- 433 [14] D. Polarski, A. A. Starobinsky and H. Giacomini, *When is the growth index constant?*, *J.*
434 *Cosmol. Astropart. Phys.* **2016**, 037 (2016), doi:[10.1088/1475-7516/2016/12/037](https://doi.org/10.1088/1475-7516/2016/12/037).
- 435 [15] L. Wang and P. J. Steinhardt, *Cluster abundance constraints for cosmological models with a*
436 *time-varying, spatially inhomogeneous energy component with negative pressure*, *ApJ* **508**,
437 483 (1998), doi:[10.1086/306436](https://doi.org/10.1086/306436).
- 438 [16] S. Nesseris and L. Perivolaropoulos, *Testing Λ CDM with the growth function $\delta(a)$: Current*
439 *constraints*, *Phys. Rev. D* **77**, 023504 (2008), doi:[10.1103/PhysRevD.77.023504](https://doi.org/10.1103/PhysRevD.77.023504).
- 440 [17] M. Ishak, *The growth rate index of large scale structure as a*
441 *probe of the cause of cosmic acceleration*, *Lecture notes* (2009),
442 http://www.as.utexas.edu/texascosmo09/talks/tcn09_ishak.pdf.

- 443 [18] Y. Gong, M. Ishak and A. Wang, *Growth factor parametrization in curved space*, Phys. Rev.
444 D **80**, 023002 (2009), doi:[10.1103/PhysRevD.80.023002](https://doi.org/10.1103/PhysRevD.80.023002).
- 445 [19] E. V. Linder, *Cosmic growth history and expansion history*, Phys. Rev. D **72**, 043529 (2005),
446 doi:[10.1103/PhysRevD.72.043529](https://doi.org/10.1103/PhysRevD.72.043529).
- 447 [20] C. Di Porto, L. Amendola and E. Branchini, *Growth factor and galaxy bias from future*
448 *redshift surveys: a study on parametrizations*, Mon. Not. R. Astron. Soc. **419**, 985 (2011),
449 doi:[10.1111/j.1365-2966.2011.19755.x](https://doi.org/10.1111/j.1365-2966.2011.19755.x).
- 450 [21] G. Dvali, G. Gabadadze and M. Porrati, *4D gravity on a brane in 5D Minkowski space*, Phys.
451 Lett. B **485**, 208 (2000), doi:[10.1016/S0370-2693\(00\)00669-9](https://doi.org/10.1016/S0370-2693(00)00669-9).
- 452 [22] R. Calderon, D. Felbacq, R. Gannouji, D. Polarski and A. A. Starobinsky, *Global properties*
453 *of the growth index of matter inhomogeneities in the Universe*, Phys. Rev. D **100**, 083503
454 (2019), doi:[10.1103/PhysRevD.100.083503](https://doi.org/10.1103/PhysRevD.100.083503).
- 455 [23] N. Suzuki et al., *The hubble space telescope cluster supernova survey. V. improving the*
456 *dark-energy constraints above $z > 1$ and building an early-type-hosted supernova sample*,
457 ApJ **746**, 85 (2012), doi:[10.1088/0004-637x/746/1/85](https://doi.org/10.1088/0004-637x/746/1/85).
- 458 [24] C.-H. Chuang et al., *The clustering of galaxies in the SDSS-III baryon oscillation spectroscopic*
459 *survey: single-probe measurements from CMASS anisotropic galaxy clustering*, Mon. Not. R.
460 Astron. Soc. **461**, 3781 (2016), doi:[10.1093/mnras/stw1535](https://doi.org/10.1093/mnras/stw1535).
- 461 [25] C.-H. Chuang et al., *The clustering of galaxies in the completed SDSS-III baryon oscillation*
462 *spectroscopic survey: single-probe measurements from DR12 galaxy clustering – towards an*
463 *accurate model*, Mon. Not. R. Astron. Soc. **471**, 2370 (2017), doi:[10.1093/mnras/stx1641](https://doi.org/10.1093/mnras/stx1641).
- 464 [26] Y. Wang et al., *The clustering of galaxies in the completed SDSS-III baryon oscillation*
465 *spectroscopic survey: tomographic BAO analysis of DR12 combined sample in configuration*
466 *space*, Mon. Not. R. Astron. Soc. **469**, 3762 (2017), doi:[10.1093/mnras/stx1090](https://doi.org/10.1093/mnras/stx1090).
- 467 [27] Y. Wang, G.-B. Zhao, C.-H. Chuang, M. Pellejero-Ibanez, C. Zhao, F.-S. Kitaura and
468 S. Rodriguez-Torres, *The clustering of galaxies in the completed SDSS-III baryon oscil-*
469 *lation spectroscopic survey: a tomographic analysis of structure growth and expansion*
470 *rate from anisotropic galaxy clustering*, Mon. Not. R. Astron. Soc. **481**, 3160 (2018),
471 doi:[10.1093/mnras/sty2449](https://doi.org/10.1093/mnras/sty2449).
- 472 [28] G.-B. Zhao et al., *The clustering of galaxies in the completed SDSS-III baryon oscillation*
473 *spectroscopic survey: tomographic BAO analysis of DR12 combined sample in Fourier space*,
474 Mon. Not. R. Astron. Soc. **466**, 762 (2016), doi:[10.1093/mnras/stw3199](https://doi.org/10.1093/mnras/stw3199).
- 475 [29] A. J. Cuesta et al., *The clustering of galaxies in the SDSS-III baryon oscillation spec-*
476 *troscopic survey: baryon acoustic oscillations in the correlation function of LOWZ and*
477 *CMASS galaxies in data release 12*, Mon. Not. R. Astron. Soc. **457**, 1770 (2016),
478 doi:[10.1093/mnras/stw066](https://doi.org/10.1093/mnras/stw066).
- 479 [30] H. Gil-Marín et al., *The clustering of the SDSS-IV extended baryon oscillation spectroscopic*
480 *survey DR14 quasar sample: structure growth rate measurement from the anisotropic quasar*
481 *power spectrum in the redshift range $0.8 < z < 2.2$* , Mon. Not. R. Astron. Soc. **477**, 1604
482 (2018), doi:[10.1093/mnras/sty453](https://doi.org/10.1093/mnras/sty453).
- 483 [31] S. Alam et al., *The clustering of galaxies in the completed SDSS-III baryon oscillation*
484 *spectroscopic survey: cosmological analysis of the DR12 galaxy sample*, Mon. Not. R. Astron.
485 Soc. **470**, 2617 (2017), doi:[10.1093/mnras/stx721](https://doi.org/10.1093/mnras/stx721).

- 486 [32] F. Beutler et al., *The clustering of galaxies in the completed SDSS-III baryon oscillation*
487 *spectroscopic survey: baryon acoustic oscillations in the Fourier space*, Mon. Not. R. Astron.
488 Soc. **464**, 3409 (2016), doi:[10.1093/mnras/stw2373](https://doi.org/10.1093/mnras/stw2373).
- 489 [33] M. Vargas-Magaña et al., *The clustering of galaxies in the completed SDSS-III baryon*
490 *oscillation spectroscopic survey: theoretical systematics and baryon acoustic oscillations*
491 *in the galaxy correlation function*, Mon. Not. R. Astron. Soc. **477**, 1153 (2018),
492 doi:[10.1093/mnras/sty571](https://doi.org/10.1093/mnras/sty571).
- 493 [34] G. C. Carvalho, A. Bernui, M. Benetti, J. C. Carvalho and J. S. Alcaniz, *Baryon acoustic*
494 *oscillations from the SDSS DR10 galaxies angular correlation function*, Phys. Rev. D **93**,
495 023530 (2016), doi:[10.1103/PhysRevD.93.023530](https://doi.org/10.1103/PhysRevD.93.023530).
- 496 [35] D. Wang et al., *The clustering of the SDSS-IV extended baryon oscillation spectroscopic*
497 *survey DR14 quasar sample: anisotropic baryon acoustic oscillations measurements in*
498 *Fourier-space with optimal redshift weights*, Mon. Not. R. Astron. Soc. **477**, 1528 (2018),
499 doi:[10.1093/mnras/sty654](https://doi.org/10.1093/mnras/sty654).
- 500 [36] F. Zhu et al., *The clustering of the SDSS-IV extended baryon oscillation spectroscopic survey*
501 *DR14 quasar sample: measuring the anisotropic baryon acoustic oscillations with redshift*
502 *weights*, Mon. Not. R. Astron. Soc. **480**, 1096 (2018), doi:[10.1093/mnras/sty1955](https://doi.org/10.1093/mnras/sty1955).
- 503 [37] G.-B. Zhao et al., *The clustering of the SDSS-IV extended baryon oscillation spectroscopic*
504 *survey DR14 quasar sample: a tomographic measurement of cosmic structure growth and*
505 *expansion rate based on optimal redshift weights*, Mon. Not. R. Astron. Soc. **482**, 3497
506 (2018), doi:[10.1093/mnras/sty2845](https://doi.org/10.1093/mnras/sty2845).
- 507 [38] H. Gil-Marín, W. J. Percival, L. Verde, J. R. Brownstein, C.-H. Chuang, F.-S. Kitaura,
508 S. A. Rodríguez-Torres and M. D. Olmstead, *The clustering of galaxies in the SDSS-III*
509 *baryon oscillation spectroscopic survey: RSD measurement from the power spectrum and*
510 *bispectrum of the DR12 BOSS galaxies*, Mon. Not. R. Astron. Soc. **465**, 1757 (2016),
511 doi:[10.1093/mnras/stw2679](https://doi.org/10.1093/mnras/stw2679).
- 512 [39] P. Zarrouk et al., *The clustering of the SDSS-IV extended baryon oscillation spectroscopic*
513 *survey DR14 quasar sample: measurement of the growth rate of structure from the anisotropic*
514 *correlation function between redshift 0.8 and 2.2*, Mon. Not. R. Astron. Soc. **477**, 1639
515 (2018), doi:[10.1093/mnras/sty506](https://doi.org/10.1093/mnras/sty506).
- 516 [40] E. de Carvalho, A. Bernui, G. C. Carvalho, C. P. Novaes and H. S. Xavier, *Angular baryon*
517 *acoustic oscillation measure at $z = 2.225$ from the SDSS quasar survey*, J. Cosmol. Astropart.
518 Phys. **2018**, 064 (2018), doi:[10.1088/1475-7516/2018/04/064](https://doi.org/10.1088/1475-7516/2018/04/064).
- 519 [41] J. E. Bautista et al., *Measurement of baryon acoustic oscillation correlations at $z = 2.3$ with*
520 *SDSS DR12 Ly α -Forests*, A&A **603**, A12 (2017), doi:[10.1051/0004-6361/201730533](https://doi.org/10.1051/0004-6361/201730533).
- 521 [42] T. Delubac et al., *Baryon acoustic oscillations in the Ly α forest of BOSS DR11 quasars*, A&A
522 **574**, A59 (2015), doi:[10.1051/0004-6361/201423969](https://doi.org/10.1051/0004-6361/201423969).
- 523 [43] H. du Mas des Bourboux et al., *Baryon acoustic oscillations from the complete SDSS-III Ly α -*
524 *quasar cross-correlation function at $z = 2.4$* , A&A **608**, A130 (2017), doi:[10.1051/0004-6361/201731731](https://doi.org/10.1051/0004-6361/201731731).
- 525